Title

Local hydroclimate drives differential warming rates between regular summer days and extreme hot days in the Northern Hemisphere

Authors

Srivastava, Abhishekh Kumar
Wehner, Michael
Bonfils, Céline
et al.

Publication Date

2024-09-01

DOI

10.1016/j.wace.2024.100709

Weather and Climate Extremes 45 (2024) 100709

Contents lists available at ScienceDirect

Weather and Climate Extremes

journal homepage: www.elsevier.com/locate/wace

Local hydroclimate drives differential warming rates between regular summer days and extreme hot days in the Northern Hemisphere

Abhishekh Kumar Srivastava [a,*], Michael Wehner [b], Céline Bonfils [c], Paul Aaron Ullrich [a,c], Mark Risser [d]

[a] Department of Land, Air and Water Resources, University of California, Davis, CA, USA
[b] Applied Mathematics and Computational Research Division, Lawrence Berkeley National Laboratory, Berkeley, CA, USA
[c] Lawrence Livermore National Laboratory, Livermore, CA, USA
[d] Climate and Ecosystem Sciences Division, Lawrence Berkeley National Laboratory, Berkeley, CA, USA

ARTICLE INFO

Dataset link: https://www.ecmwf.int/en/forecasts/dataset/ecmwf-reanalysis-v5, https://www.cesm.ucar.edu/community-projects/lens

Keywords:
Temperature extremes
Extreme heat
Warming
Land–climate interactions
Hydroclimate
ERA5
CESM1-LE

ABSTRACT

In this work, we compare the rate of warming of summertime extreme temperatures (summer maximum value of daily maximum temperature; TXx) relative to the local mean (summer mean daily maximum temperature; TXm) over the Northern Hemisphere in observations and one set of large ensemble (LE) simulations. During the 1979–2021 historical period, observations and simulations show robust warming trends in both TXm and TXx almost everywhere in the Northern Hemisphere, except over the eastern U.S. where observations show a slight cooling trend in TXx, which may be a manifestation of internal variability. We find that the observed warming rate in TXx is significantly smaller than in TXm in North Africa, western North America, Siberia, and Eastern Asia, whereas the warming rate in TXx is significantly larger over the Eastern U.S., the U.K., and Northwestern Europe. This observed geographical pattern is successfully reproduced by the vast majority of the LE members over the historical period, and is persistent (although less intense) in future climate projections over the 2051–2100 period. We also find that these relative warming patterns are mostly driven by the local hydroclimate conditions. TXx warms slower than TXm in the hyper-arid, arid, semi-arid and moist regions, where trends in the partitioning of the turbulent surface fluxes between the latent and sensible heat flux are similar during regular and extreme hot days. In contrast, TXx warms faster than TXm in dry-subhumid regions where trends in the partitioning of the surface fluxes are significantly different between regular and extreme hot days, with a larger role of sensible heat flux during the extreme hot days.

1. Introduction

Hot extremes pose challenges for different sectors of society and economy, such as human health (Ebi et al., 2021; Lian et al., 2023), animal discomfort (Wankar et al., 2021), agriculture (Miller et al., 2021), and energy (Miller et al., 2008). Backed by a strong scientific foundation (Alexander et al., 2006; Diffenbaugh and Ashfaq, 2010; Christidis et al., 2011; Zwiers et al., 2011; Perkins et al., 2012; Min et al., 2013; Diffenbaugh et al., 2017; Vose et al., 2017; Wehner et al., 2018b; Byrne, 2021; Li et al., 2021), the sixth Assessment Report (AR6) of the Intergovernmental Panel on Climate Change (IPCC) reports with certainty that global warming has increased the frequency and intensity of heat extremes, and even small incremental warming by 0.5 °C of global mean temperature can cause a statistically significant increase in temperature extremes on the global scale and large regions (*very likely*) (Seneviratne et al., 2021). But will summer hot days warm at a faster rate than regular summer days? To address this question, several studies have compared the warming of hot extremes against the warming of the mean (global and local) temperatures (e.g., McKinnon et al., 2016; Seneviratne et al., 2016; Donat et al., 2017; Vogel et al., 2017; Wehner et al., 2018a; Di Luca et al., 2020; Duan et al., 2020; Byrne, 2021; Wang et al., 2022; Krakauer, 2023; Patterson, 2023). However, the answer to this question is not straightforward for at least two reasons: (i) because of how physical processes and their interactions, such as large-scale atmospheric circulation patterns (Meehl and Tebaldi, 2004; Diffenbaugh and Ashfaq, 2010; Miralles et al., 2014; Patterson, 2023) and land–atmosphere interactions (e.g., soil moisture-evaporation-temperature feedback; Seneviratne et al., 2010; Whan et al., 2015; Donat et al., 2017; Vogel et al., 2017; Miralles et al., 2019), drive temperature extremes at varied temporal and regional scales; and (ii) because results strongly depend upon factors such as

* Corresponding author.
E-mail address: asrivas@ucdavis.edu (A.K. Srivastava).

https://doi.org/10.1016/j.wace.2024.100709
Received 28 September 2023; Received in revised form 20 July 2024; Accepted 28 July 2024
Available online 30 July 2024

timescales, seasons, regions, metrics, and thresholds (Lewis and King, 2017; Di Luca et al., 2020; Duan et al., 2020).

There is now enough evidence to suggest that, on global and continental scales, warming of heat extremes is significantly faster than warming of the global mean temperature (e.g., Seneviratne et al., 2021; Philip et al., 2022). However, there are regional disparities in the trends of extreme temperatures against trends in both the local and global mean. For example, a few studies suggest that the hot extremes have warmed faster than the global mean temperature in many parts of the world, including Europe, the Mediterranean region, and South America (Seneviratne et al., 2016; Vogel et al., 2017; Philip et al., 2022). On the other hand, previous studies also indicate that the annual maximum temperatures over eastern North America are increasing slower than the mean temperatures (Philip et al., 2022; Patterson, 2023). Donat et al. (2017) found that the observed changes in the annual maximum temperature are smaller than the local annual average temperature almost everywhere in the Northern Hemisphere, except northeastern Canada and Europe. Patterson (2023) found that the observed changes in the JJA maximum of the daily maximum temperature are not statistically different from the local mean JJA daily maximum temperature in many areas of the Northern Hemisphere, except northwestern Europe and sporadic regions of Siberia. Recently, Duan et al. (2020) analyzed the Climate Model Intercomparison Project Phase 5 (CMIP5) model simulations and showed that, in response to a quadrupling of CO_2, the largest 20% of the simulated summertime daily maximum temperatures increase more than the corresponding mean over moist land regions, whereas extremes increase less than the mean over dry land regions.

The above studies provide valuable insight into how hot extremes respond to climate change in comparison to the mean temperatures. Nevertheless, the question of the warming of hot extremes relative to the mean is complex. For example, results based on the comparison of the warming of annual temperature extremes against the warming of the annual mean (e.g., Donat et al., 2017) cannot be extrapolated to seasonal extremes. Second, most of the multimodel ensemble-based studies analyzing changes in hot extremes against the local/global mean find that the models are often inconsistent with observations (e.g., Donat et al., 2017; Patterson, 2023). In such multimodel ensemble-based studies, it is difficult to separate internal variability from model errors (Tebaldi et al., 2011; Kay et al., 2015). Li et al. (2021) demonstrated that large ensemble simulations, enabling the increased sampling of internal climate variability, can robustly project future changes in climate extremes at small spatial scales. Third, almost all of the previous studies address the question of the warming of extremes relative to the mean by focusing on trends in the two quantities. Since extremes and mean are described by different distributions, comparing their linear trends may be problematic in a few regions, especially in places where trends are small and statistically insignificant.

With the aim of addressing limitations from these previous studies, we investigate the question of the warming of the extreme temperatures relative to the local mean in a statistically rigorous manner. To this end, we apply a generalized extreme value (GEV) distribution framework to compare changes in the summertime (June/July/August or JJA) maximum (TXx) of the daily maximum temperatures relative to the corresponding local JJA mean (TXm) daily maximum temperatures. We focus on the summertime mean and extreme temperatures because warming patterns of the mean temperatures differ by season and because summertime heatwaves are the most impactful to human and natural ecosystems. We use large ensemble simulations of the Community Earth System Model version 1 (CESM1-LE) to remove the effect of model errors from our results. We explain our results by using trends in the surface turbulent fluxes driven by the local hydroclimate conditions. Specifically, we address the following questions in this study:

1. Does CESM1-LE simulate the observed warming/ cooling trends in the summertime TXm and TXx over the northern hemisphere (NH)?
2. Are the observed cooling trends in the summertime TXx (hereafter defined as the *warming hole*) over the eastern CONUS a manifestation of internal climate variability?
3. Are the observed warming trends in TXx larger or smaller than those in the local TXm during the historical period? Can the CESM1-LE reproduce observations?
4. How do the competing trends in TXx and TXm change in the future?
5. Do trends in surface fluxes driven by the local hydroclimate explain the warming of extreme temperatures relative to the mean?

We hypothesize that the warming of the TXx relative to the TXm can be explained by trends in the partitioning of the surface turbulent fluxes into latent and sensible heat.

The remainder of the paper is as follows. Section 2 describes the data and methods used in the study. Results are discussed in Section 3 and summarized in Section 4.

2. Data and methods

As a proxy for observed global temperatures, we use ERA5 reanalysis data over the period 1979–2021 (Hersbach et al., 2020). For model analysis, we use historical and RCP8.5 simulations of the CESM1-LE (Kay et al., 2015). The CESM1-LE consists of 40 ensemble members from the fully-coupled CESM1 simulations of the historical and future climate for the period 1920–2100. Each ensemble member uses the same radiative forcing scenario for the historical (1920–2005) and RCP8.5 (2006–2100) periods but starts from a slightly different initial atmospheric state. To allow a direct comparison of observed and simulated changes over the entire reanalysis period, we concatenated the CESM1-LE historical simulations for the 1979–2005 period with their corresponding RCP8.5 simulations for the 2005–2021 period. For estimation of future warming trends, we use the 2051–2100 period from the RCP8.5 simulations. We focus on the boreal summer season (JJA) over the regions bounded between 20°N-90°N in the Northern Hemisphere. We emphasize that we selected RCP8.5, regarded as an "unlikely worst case" (Hausfather and Peters, 2020) to explore the persistence of mechanisms driving differential warming rates of TXx and TXm in an extreme scenario. Despite criticisms, RCP8.5 provides an opportunity to understand the risks posed by climate extremes (Tollefson, 2020). Arguably, the timing of global warming on RCP8.5 may be early, but without zero emissions, these temperatures will eventually be reached and surpassed.

For mean warming (TXm), we use the Northern Hemisphere summer (JJA) seasonal means of the daily maximum 2 m temperature (2t) over 1979–2021 (43 years) in ERA5 and the maximum reference height temperature (TREFHTMX) in the CESM1-LE simulations. For extreme warming (TXx), we use the JJA maxima of the daily 2 m temperature in ERA5 and the daily TREFHTMX in CESM1-LE. For convenience, we denote the JJA mean daily maximum temperatures as TXm and the overall JJA maxima as TXx. We investigate the warming of the hot extremes relative to the local mean using the generalized extreme value (GEV) distribution framework. The GEV distribution has three parameters: location (μ), scale (σ) and shape (ζ). We use the local JJA mean daily maximum temperature (TXm) as a covariate in the location parameter of the TXx GEV distribution:

$$\mu_{\mathrm{TXx}} = \mu_0 + \mu_1 \mathrm{TXm}, \tag{1}$$

where μ_{TXx} is the location parameter of the TXx GEV distribution, μ_0 is the intercept and μ_1 is the slope of the regression Eq. (1). We keep the other two parameters (scale and shape) fixed. These four parameters of the fitted GEV distribution are estimated using the maximum-likelihood method (Coles et al., 2001). The 95% confidence interval (CI = 97.5th

(UCI) minus 2.5th (LCI) percentiles) of the fitted parameters is estimated using the parametric bootstrap method that simulates the data from the fitted distribution and then fits GEV to each simulated data to obtain samples of the parameters. We estimate the confidence intervals from 100 bootstrapped samples. If the 95% CI of μ_1 (in Eq. (1)) does not include zero, μ_1 is said to be statistically different from zero. We use the same 95% confidence interval of μ_1 to determine if TXx rises *significantly* faster or slower than TXm. If both the LCI and UCI are greater than 1, we conclude that the per °C positive change in TXx is significantly greater than the per °C positive change in TXm, i.e., the JJA extreme temperature rises faster than the local temperature mean. On the other hand, if the CI (UCI minus LCI) does not include zero, and both the LCI and UCI are less than 1, we conclude that the per °C positive change in TXx is significantly smaller than the per °C positive change in TXm, i.e., the JJA extreme temperature rises slower than the local mean temperature.

Previous studies suggest that soil moisture-evaporation-temperature feedback is the highly relevant mechanism for the amplification and persistence of warm extremes (Benson and Dirmeyer, 2021; Seneviratne et al., 2010; Whan et al., 2015; Duan et al., 2020). We examine the local surface conditions on the day when the TXx occurs. Therefore, we use the CESM1-LE soil moisture, sensible, and latent heat fluxes on the day when TXx occurs. All fields are interpolated to the CESM1-LE grid using the first-order conservative remapping (Jones, 1999).

3. Results

3.1. Local trends in TXx and TXm

The first objective of this manuscript is to show that CESM1-LE is consistent with ERA5, our proxy for globally complete observations. Fig. 1 shows trends in JJA extreme (TXx) and mean (TXm) temperatures over 1979–2021 in the Northern Hemisphere (NH) in ERA5. As reported in previous studies (e.g., Alexander et al., 2006; Cohen et al., 2012; Dunn et al., 2020; Seneviratne et al., 2021; Patterson, 2023), both TXx and TXm show significant warming trends over most of the NH. Warming trends are strongest over Europe, Western North America and Greenland. In contrast to ubiquitous warming trends in TXm over land, TXx exhibits cooling trends (also known as the warming hole) over a few regions, most notably over the eastern CONUS (ECONUS), Kazakhstan, and India. The reason for the ECONUS warming hole is not clear, and possible causes include internal climate variability (e.g., Kunkel et al., 2006; Partridge et al., 2018; Sun et al., 2022), external forcing (e.g., sulfate aerosols; Leibensperger et al., 2012), irrigation practices (Thiery et al., 2017), and land use changes (Cowan et al., 2020).

Fig. 2 (a & b) show the ensemble median trends in TXx and TXm in the CESM1-LE simulations over 1979–2021. Overall, the CESM1-LE exhibits warming trends in both the mean and extreme temperatures everywhere. The warming trend is stronger over central North America, Europe, and Northern Siberian regions. Unsurprisingly, none of the TXx cooling trends observed in ERA5 appear in the CESM1-LE TXx ensemble median trend, corroborating results from previous multimodel ensemble mean trend estimates (e.g., Kunkel et al., 2006; Donat et al., 2017). Fig. 2 (c & d) show trends in TXm and TXx over 2051–2100 in RCP8.5. CESM1-LE projects much-accelerated warming of both the mean and extreme temperatures over 2051–2100 in RCP8.5 as compared to 1979–2021, consistent with previous studies (Seneviratne and Hauser, 2020; Wehner, 2020).

Regarding the TXx trends from ERA5 and CESM1-LE, it is natural to ask whether or not the model simulated warming of TXx during 1979–2021 is consistent with the TXx warming hole in ERA5. This question is also interesting, as previous studies (e.g., Donat et al., 2017) note that the CMIP5 multimodel mean simulated accelerated warming is inconsistent with observations. We address this question in two steps: First, we investigate if individual ensemble members reproduce the warming hole observed in ECONUS during 1979–2021. Second, we investigate if the CESM1-LE simulated cooling trend is consistent in area with that in ERA5. Our investigation of TXx trends in CESM1-LE indicates that around 10 out of 40 ensemble members exhibit TXx cooling trends over ECONUS; and that ensemble member #28 exhibits a TXx warming hole similar to that in ERA5 (Supplemental Fig. S1). Our results confirm that the TXx cooling trend in ERA5 may be (among other plausible causes) a strong manifestation of internal variability (arising from a backdrop of forced changes) that is averaged out when the ensemble mean trend is computed. In the second step, we compute the fractional area of negative TXx trends in ERA5 and each CESM1-LE ensemble over 1979–2021. Fig. 3 shows the histogram of the fractional area of negative TXx trends in the CESM1-LE over 1979–2021. The figure shows that the fractional area of negative TXx trends in ERA5 is above the mean but well within the 95th percentile of the fractional area of negative TXx trends in CESM1-LE ensembles. Thus our investigation suggests that CESM1-LE simulates the negative trends in TXx consistent with ERA5, but the location of the negative trends is randomly distributed over space across the CESM1-LE ensemble members.

3.2. TXx versus TXm warming in ERA5

The question of whether hot extremes are changing faster or slower than the local mean temperatures has been addressed before (e.g., Donat et al., 2017; Patterson, 2023). However, these previous studies addressed the question by applying simple measures such as differences (or the ratio) of changes in extreme temperatures minus (or over) mean temperatures. It is not clear if such simplified measures are powerful enough to elucidate different warming rates, especially in regions where changes are too small (within the significance range), as the mean and extreme temperatures follow completely different distributions. We address this question by fitting the local TXm as a covariate in the location parameter of the GEV distribution of TXx, as shown in Eq. (1).

Fig. 4 shows the regression of the location parameter of TXx on the local TXm in ERA5. Blue colors show grid points where per °C change in TXx is smaller in magnitude than the per °C positive change in the local TXm ($0 < \mu_1 < 1$). Red colors show grid points where per °C positive change in TXx is bigger than the per °C positive change in the local TXm ($\mu_1 > 1$). Notably, over most parts of the NH, the regression parameter is less than 1, suggesting that the extreme temperature is rising slower than the corresponding summer mean temperature. Particularly, western CONUS, Greenland, the Siberian region, and parts of central and western Asia are prominent land regions where the trend in summertime TXx is smaller than the local summertime TXm trend. In contrast, the eastern CONUS, the U.K., and Northwestern Europe (France, Belgium, Netherlands) are the NH regions where TXx is rising faster than the local TXm. The regional warming pattern of TXx relative to the local TXm shown in Fig. 4 has some resemblance with the corresponding patterns shown in previous research. For example, the faster warming of TXx over western Europe and the slower warming over western CONUS and the northern parts of Siberia have also been shown by Donat et al. (2017) and Patterson (2023). However, no previous research showed a faster warming trend of TXx over eastern CONUS, as appears in Fig. 4.

The results for ECONUS are counterintuitive because TXm has a small positive trend while TXx has a small negative trend over the eastern CONUS in the ERA5 reanalysis (Fig. 1). We argue that simple measures, such as the difference or ratio of the two trends, may not be able to quantify the true nature of relative changes in extremes over the mean, especially in locations where the trends are too small. This point is further illustrated in the Supplemental Fig. S2 . The black dots in the figure show the grid points where TXm has a positive trend (panel a), and TXx has a negative trend (panel b). Therefore, the difference between trends in TXx and TXm (trend in TXx minus trend in TXm) is negative (panel c). When the individual TXx and TXm trends are small

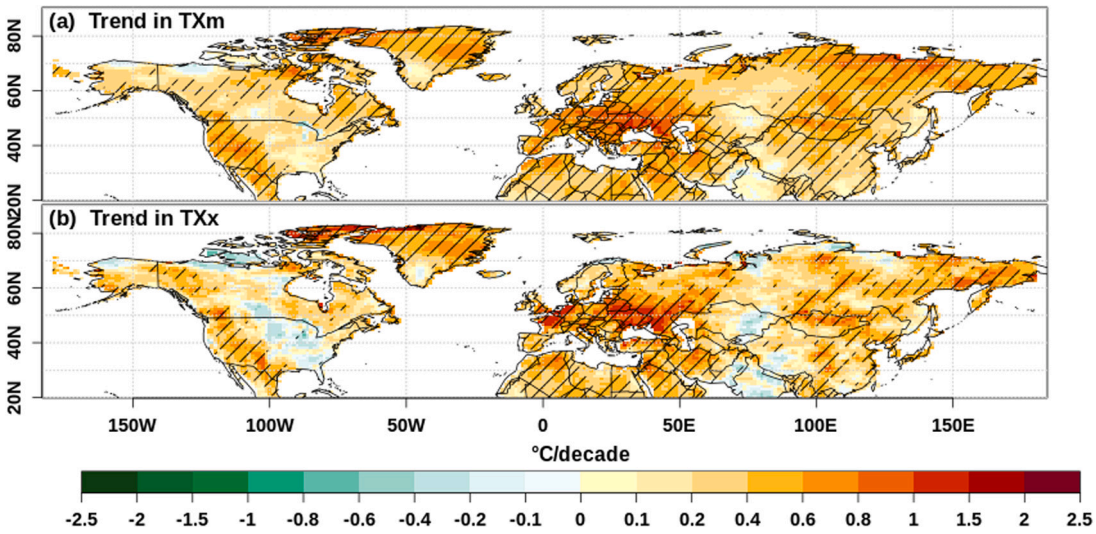

Fig. 1. Trend (°C/decade) in TXx and TXm computed using Sen's slope over 1979–2021 in ERA5. Hatchings show trends significant at the 5% level.

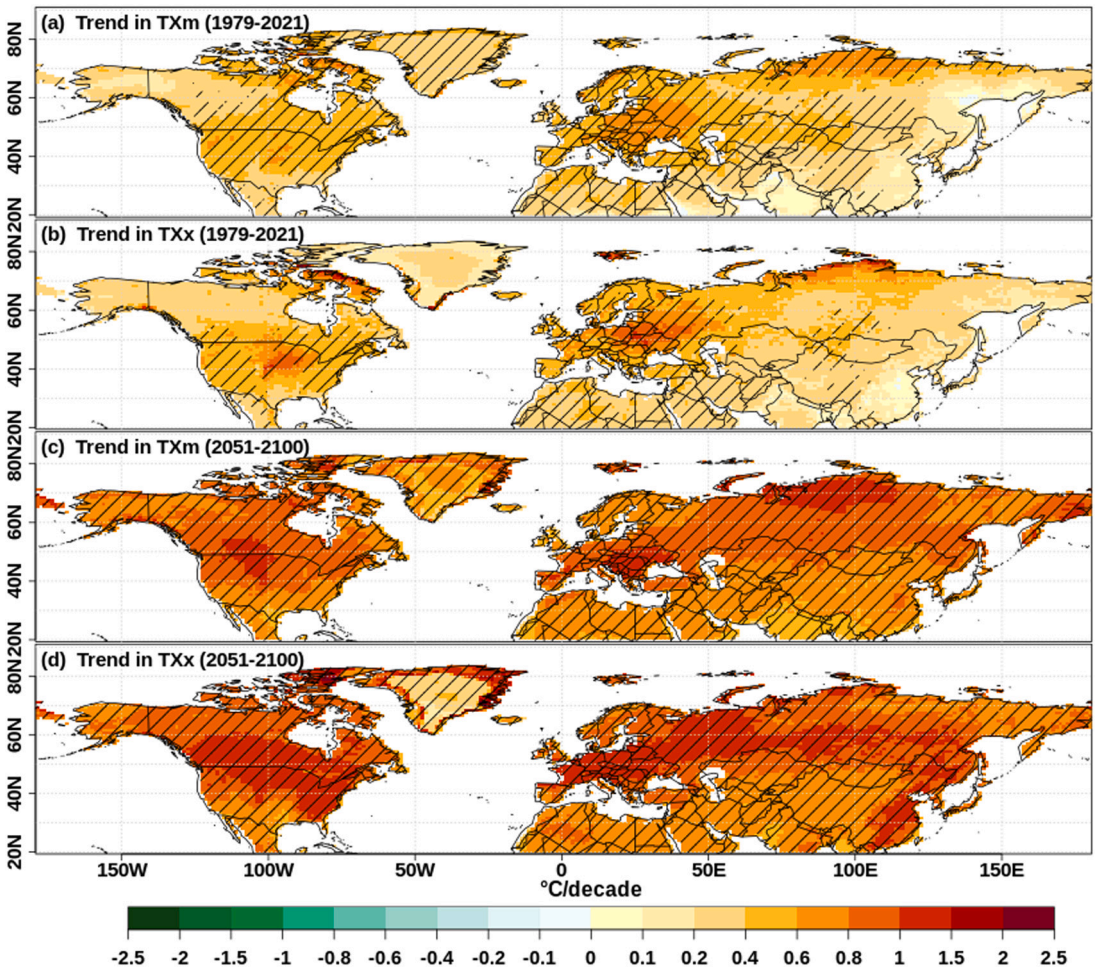

Fig. 2. Ensemble median trend (°C/decade) in TXx and TXm computed using Sen's slope over 1979–2021 in CESM1-LE. Hatchings show grid points where trends are significant at the 5% level in at least 20 out of 40 ensemble members.

relative to the uncertainty, apparent contradictions can arise between trend estimates and the relative behavior of TXx as a function of TXm. For example, consider the grid points marked by black dots in Fig. S2, where the regression coefficients are greater than 1 (panel d), yet the TXx trends are slightly negative (panel b) but the TXm trends are slightly positive (panel a). These contradictory behaviors occur in intermediate regions in terms of the local hydroclimatic processes as discussed in Sections 3.4 and 3.5.

To investigate the hypothesis that TXx may *actually* be rising faster than TXm even if TXx has a small negative and TXm has a small positive

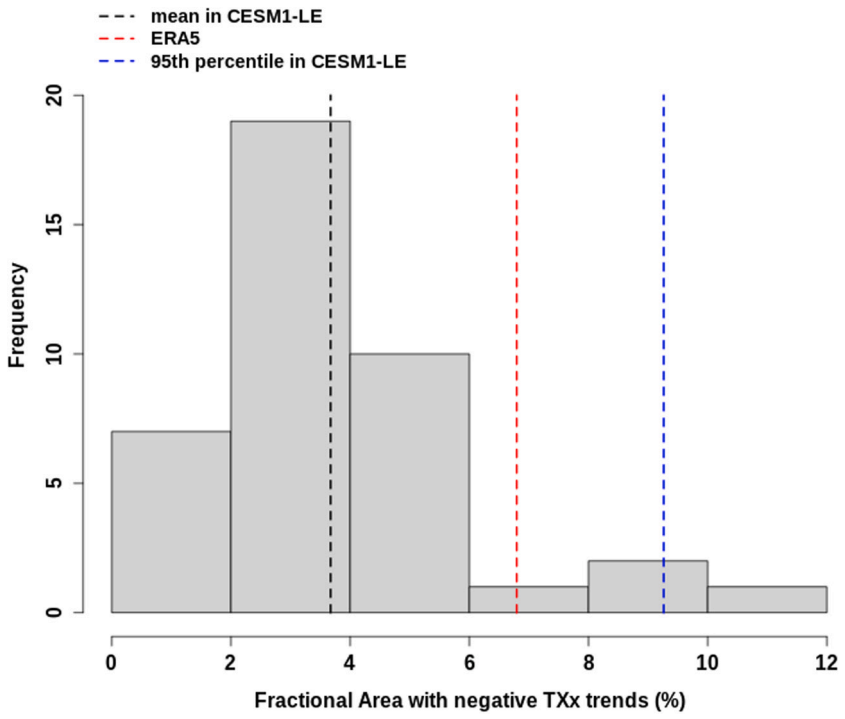

Fig. 3. Histogram of the fractional area of negative TXx trends in CESM1-LE. The black dashed line shows the mean fractional area with a negative TXx trend in CESM1-LE. The red dashed line indicates the fractional area with a negative TXx trend in ERA5. The blue dashed line shows the 95th percentile of the fractional area in CESM1-LE. Unit: %.

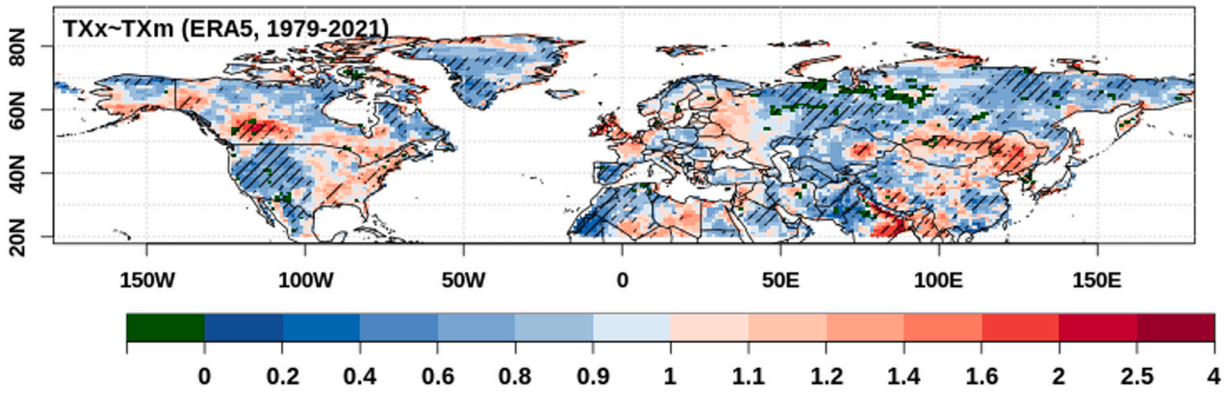

Fig. 4. Regression of the location parameter of TXx on the local TXm in ERA5. The red (blue) colors show grid points where per °C positive change in TXx is bigger (smaller) than the per °C positive change in the local TXm over 1979–2021. Green shading shows regions where per °C change in TXx is negative for per °C positive change in the local TXm. The hatching shows grid points where the regression parameter is significant at 5%. Unit: °C/°C. (For interpretation of the references to color in this figure legend, the reader is referred to the web version of this article.)

trend, we perform a statistical test at a location (Longitude: 96.25°W, Latitude: 42.9°N) in the ECONUS (the black circle in the Supplemental Fig. S2) that has a significant negative trend in TXx and a positive trend in TXm in ERA5 (Supplemental Fig. S3). The statistical test has the following steps:

1. Estimate the parameters (location, scale, and shape) of the GEV distribution of TXx (actual data) whose location parameter is modeled as: $\mu_{TXx\sim TXm} = \mu_0 + \mu_1 TXm$.
2. Generate a random sample with the length equal to the number of data points (sampled data) from the distribution that has the same parameters as in step 1.
3. Estimate the slope of the location parameter (μ_1) for the sampled data, similar to step 1.
4. Estimate the trend in the sampled data.
5. Repeat steps 2–4 100 times.

It is apparent from Fig. 5 that there are a significantly large number (31%) of bootstrapped samples for which TXx is rising faster than TXm (solid green squares) even though TXx may have a small negative trend (solid red square) and TXm has a small positive trend (in 36% samples μ_1 is still positive but less than 1). Nonetheless, to make sure that the results shown in Fig. 4 are not an artifact of the GEV distribution involved, we also perform a linear regression analysis (Supplemental Fig. S4), in which TXx is linearly regressed on the local TXm over the CONUS. We find that the spatial pattern of the regression parameter obtained from the simple linear regression is similar to that obtained from the GEV distribution analysis as in Fig. 4.

3.3. TXx versus TXm warming in CESM1-LE

Fig. 6(a) shows the ensemble-median regression of the location parameter of TXx on the local TXm in CESM1-LE for the 1979–2021 period. Blue (red) shading shows the regions where $0 < \mu_1 < 1$ ($\mu_1 > 1$),

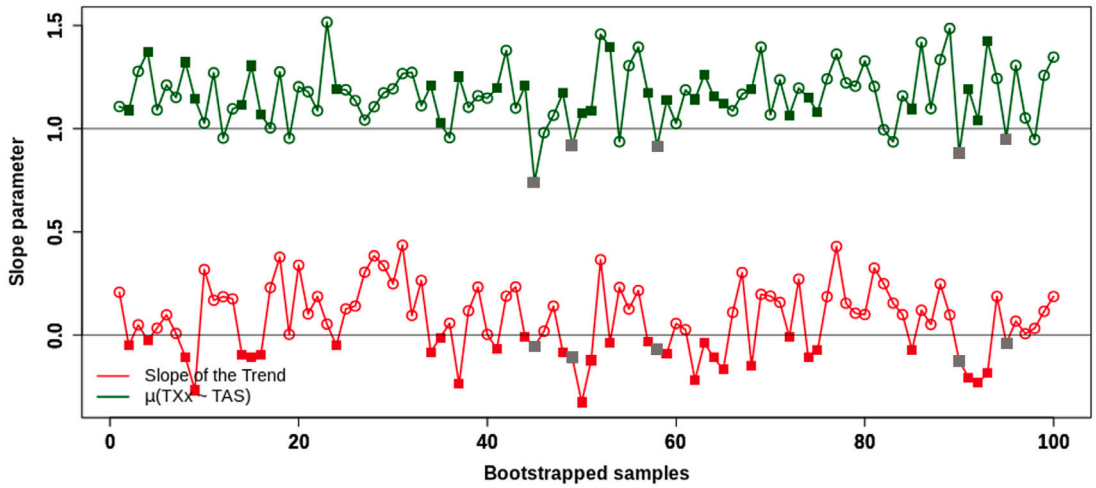

Fig. 5. Results of a statistical test performed at the selected location (Longitude: 96.25°W, Latitude: 42.9°N) in the ECONUS to prove the hypothesis that the sampled TXx data may have a negative trend even when the sampled TXx is actually rising faster than the observed TXm ($\mu_1 > 1$). The red curve shows the trend in the sampled TXx. The green curve shows the change in the sampled TXx against the change in the observed TXm. μ_1 greater (smaller) than 1 indicates that the sampled TXx is rising faster (slower) than the observed TXm. The solid green and red boxes indicate the samples for which the above hypothesis is true. The solid gray boxes show the bootstrapped samples for which $0 < \mu_1 < 1$. (For interpretation of the references to color in this figure legend, the reader is referred to the web version of this article.)

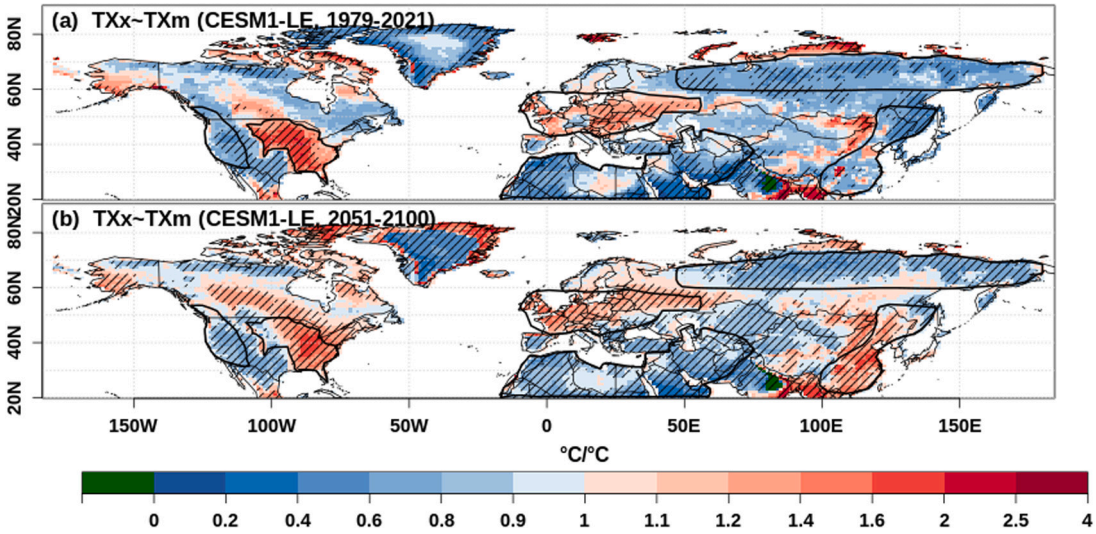

Fig. 6. Regression of the location parameter of TXx on the local TXm in CESM1-LE. The regression coefficient shown is the multi-ensemble median of the individual regression coefficient in the CESM1-LE. The red (blue) colors show grid points where per °C positive change in TXx is bigger (smaller) than the per °C positive change in the local TXm over 1979–2021 (a) and 2051–2100 (b). Green shadings show regions where per °C change in TXx is negative for per °C positive change in the local TXm. The hatchings show grid points where the regression parameter is significant at 5% in at least 20 out of 40 ensemble members. The closed polygons indicate the geographical regions analyzed in this study. Unit: °C/°C. (For interpretation of the references to color in this figure legend, the reader is referred to the web version of this article.)

indicating that TXx is rising slower (faster) than the local TXm in those regions. Consistent with the corresponding pattern in ERA5 (Fig. 4), the CESM1-LE shows that over most of the NH land, TXx is rising slower than TXm. Eastern North America and Western and Central Europe are the regions where the rate of TXx warming is faster than that of TXm. It is worth noting that the ensemble median pattern shown in Fig. 6 is a robust feature of the CESM1-LE because the pattern is present in at least 36 out of 40 ensemble members. Nonetheless, a striking similarity of Figs. 4 and 6 indicates that the observed warming/ cooling of TXx relative to the local TXm is not due to the internal variability and is a robust feature of the climate system.

Future warming of Txx relative to the local TXm over 2051–2100 in RCP8.5 is shown in Fig. 6(b). The spatial pattern of the future warming/ cooling of TXx relative to TXm is *broadly* similar to that during 1979–2021. However, compared to 1979–2021, the enhanced warming of TXx relative to TXm is extended over central and western Canada, northern Europe, and East Asia in the end-of-the-century simulations. A comparison of Figs. 6(a) and (b) suggests that the regional pattern of the TXx warming relative to the local TXm warming is robust and remains more or less intact throughout the end of the 21st century RCP8.5 simulation.

3.4. Connection between the local hydroclimate and warming of TXx relative to TXm

Duan et al. (2020) showed that changes in the extreme temperatures relative to the mean depend upon the local hydroclimate, with extremes changing more than the mean in moist land regions and less than the mean in dry land regions. Following Duan et al. (2020), we compute the Aridity Index (AI), defined as $0.8R_{net}/L_v P_r$, where R_{net} is the net radiation (longwave + shortwave) at the surface, P_r is the precipitation, and L_v is the latent heat of vaporization. An AI value of more than 10 indicates a dry, less than 1 indicates a moist, and between 1 and 10 indicates an intermediate hydroclimate. The spatial pattern of the

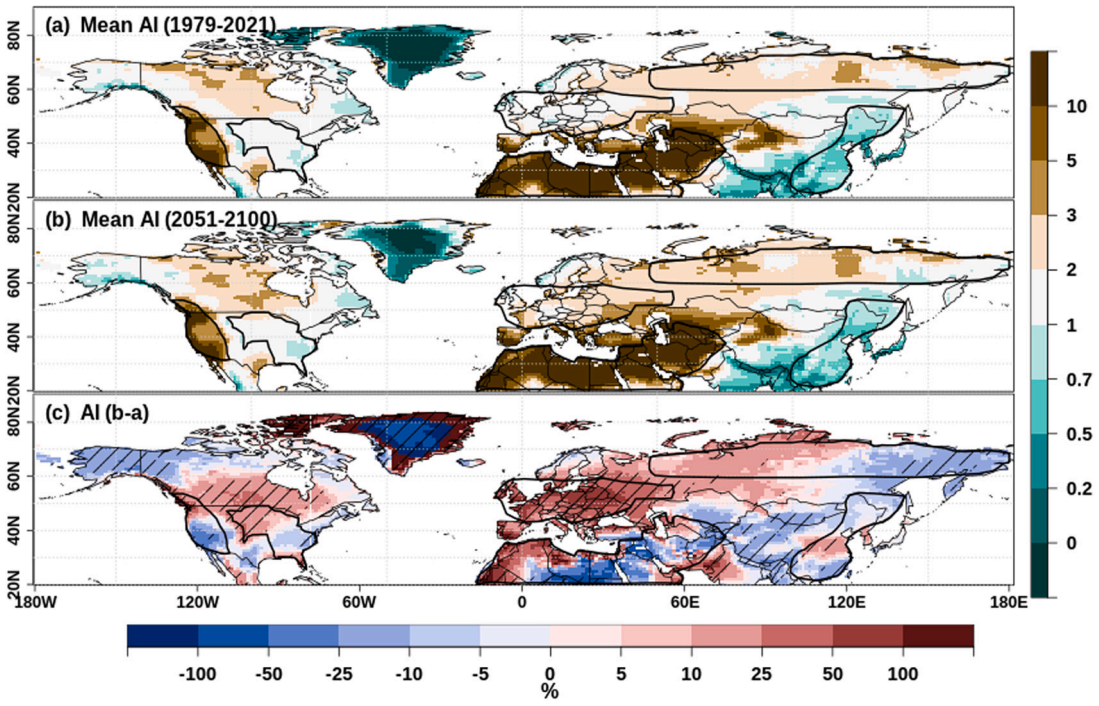

Fig. 7. Multiensemble median Aridity Index (AI) in CESM1-LE. Panel (a) shows the climatological mean AI over 1979–2021, panel (b) shows the climatological mean AI over 2051–2100 in RCP8.5, and panel (c) shows the AI over 2051–2100 minus the AI over 1979–2021. AI is unitless.

JJA mean AI in 1979–2021 (Fig. 7) is similar to the annual global aridity index of the CGIAR Consortium for Spatial Information (CGIAR-CSI) Global Aridity Index and Potential Evapotranspiration Climate Database v3 (Zomer et al., 2022). For convenience, we classify regions based upon the AI values, similar to the classification adopted in the CGIAR-CSI dataset: $AI > 10$ are classified as hyper-arid, $5 < AI \leq 10$ as arid, $2 < AI \leq 5$ as semi-arid, $1 < AI \leq 2$ as dry-subhumid, and $AI \leq 1$ as humid regions. Based upon this classification, we have identified 6 distinct regions: North Africa (NAf) and Western North America (WNA) are identified as hyper-arid and arid regions, respectively; Siberia (Sib) as semi-arid; Eastern CONUS (ECONUS) and Europe (EU) as dry-subhumid; and East Asia (EA) as a moist region (delineated in Fig. 7).

The ensemble-median climatological mean AI over 1979–2021 is shown in Fig. 7(a). A comparison of the figure with the relative warming pattern of TXx in Fig. 6 suggests that the warming rate of TXx relative to TXm is slower ($\mu_1 < 1$) mostly in hyper-arid, arid and semi-arid regions: the western coastal states of North America, Northern Canada, the Siberian region, and a large land region covering North Africa, the Middle East, and Central Asia. In contrast, the relatively faster warming of TXx compared to TXm occurs in the eastern CONUS, and West-Central Europe, characterized as dry-subhumid regions. Notably, the East Asian region (parts of Eastern China, the Korean peninsula, and Japan) is a wet region (AI < 1) that has TXx rising slower than the local TXm. The strong similarities between Figs. 6 and 7(a) indicate that the warming pattern of TXx relative to TXm is connected to the local hydroclimate through changes in the local soil moisture and associated surface latent and sensible heat fluxes.

The climatological mean AI for 2051–2100 in RCP8.5 (Fig. 7(b)) indicates that the spatial pattern of the AI remains roughly similar in an extreme warming future. However, as indicated by the positive change in AI (panel b-a in Fig. 7) aridity is expected to increase over central and northern Canada, Europe, and the Siberian region. The aridity changes in CESM1-LE are consistent with studies (Denissen et al., 2022; Hsu and Dirmeyer, 2023) that report a widespread shift from energy to water-limited soil moisture regimes in a warming world.

3.5. Trends in surface fluxes explain the warming of TXx relative to TXm

Fig. 8 shows the CESM1-LE climatological mean and trends in soil moisture and turbulent surface fluxes (latent and sensible heat) in the six regions that show enhanced or suppressed warming of the extreme temperature relative to the local mean temperature in Figs. 4 and 6. Climatologies and trends for soil moisture and surface fluxes are shown in columns II and III and columns IV and V, respectively. As expected, for both TXm and TXx events, the climatological soil moisture is much lower in the semi-arid, arid, and hyper-arid regions (Sib, WNA, NAf) than in the three relatively wetter regions (EA, ECONUS, EU) (column II). Consistent with these soil moisture and AI conditions, the climatological sensible heat flux is larger than the latent heat flux in semi-arid, arid and hyper-arid regions, and smaller in the more humid regions (column IV). Noticeably, the partitioning of the total turbulent surface fluxes into latent and sensible heat fluxes remains similar during the normal and extreme hot days in semi-arid, arid, and hyper-arid regions, but strongly differs in the humid regions, with more prominent latent heat flux during extreme hot days than during normal days (column IV). Enhanced latent heat flux during TXx days in dry-subhumid and humid regions (column IV) is consistent with the reduced soil moisture during those extreme hot days (column II), suggesting that higher atmospheric evaporative demand during extreme hot days leads to more drying of soil (Seneviratne et al., 2010).

Trends in surface fluxes during JJA mean and extreme hot days are shown in column V of Fig. 8. It is apparent that in the hyper-arid (NAf), arid (WNA), semi-arid (Sib), and moist (EA) regions, trends in latent and sensible heat fluxes (TXm and TXx days) are small ($< \pm 1$ W/m^2), and show little difference between normal and extreme hot days. In contrast, over dry-subhumid regions (ECONUS and EU), trends in latent heat flux change are large and positive (~ 2 W/m^2) on mean days, but large and negative on extreme hot days. Correspondingly, sensible heat flux also exhibits enhanced positive trends that are much larger on extreme days than on mean days. This suggests that in these dry-subhumid regions, the partitioning of the total turbulent heat flux towards sensible heat may increase at a higher rate during days

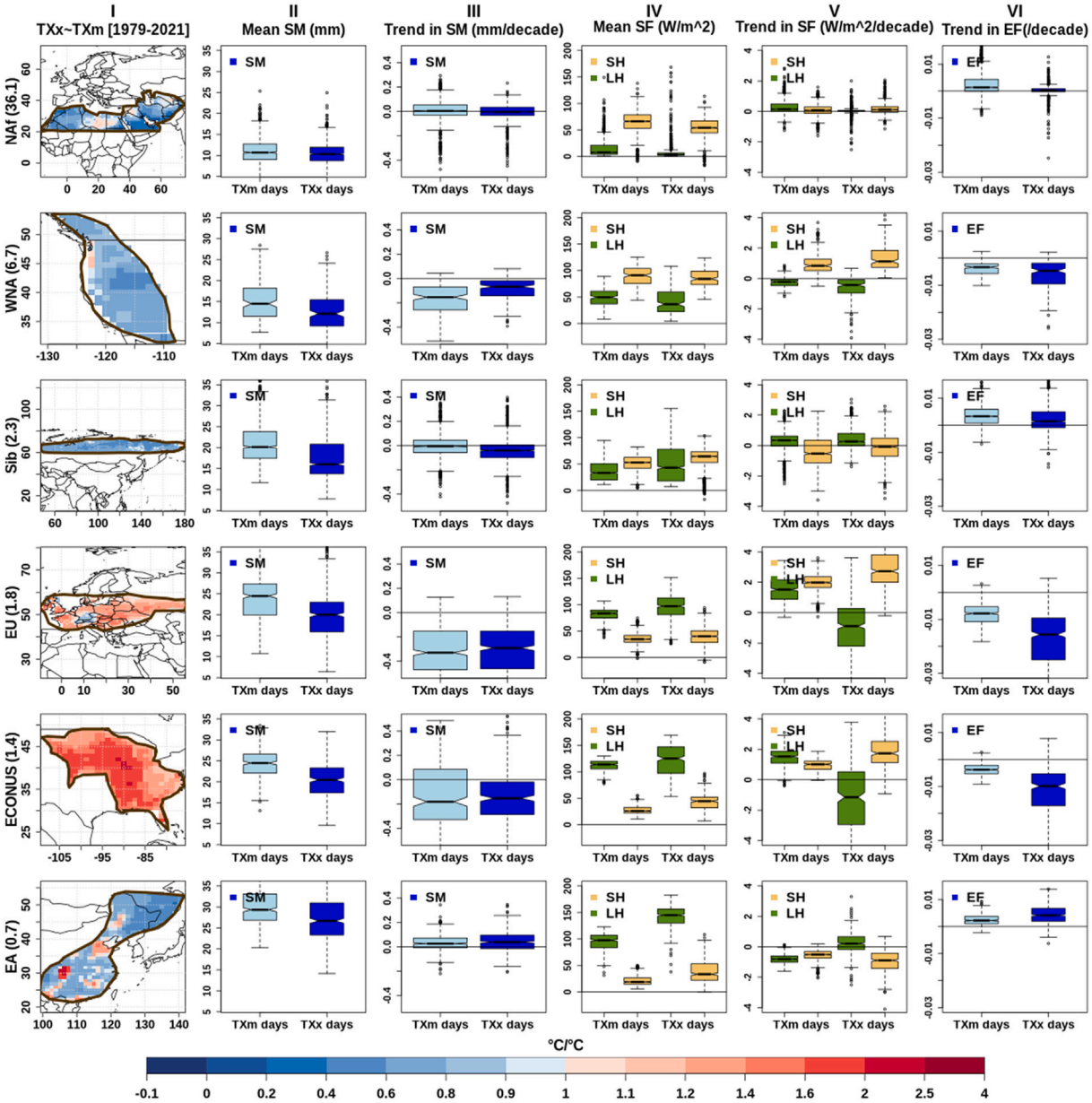

Fig. 8. Surface conditions in the CESM1-LE explaining the summertime (JJA) warming of the extreme hot days (TXx days) relative to the mean (TXm days) in 1979–2021. Each row indicates the mean conditions and trends in the surface variables for a region. Box and whiskers (BW) plots show the quantities computed at each grid point. Column I: regions where warming of extreme hot days relative to the mean are examined. The colors indicate if the warming of TXx is more (reds) or less (blues) than the local TXm. Numbers in parentheses show the median AI in that region. Column II: BW plots showing the mean soil moisture (SM) during the mean JJA season (light blue) and during the extreme hot days (dark blue). Column III: BW plots showing the trend in SM during the mean JJA season (light blue) and during the extreme hot days (dark blue). Column IV: BW plots showing the mean latent (LH) and sensible heat (SH) fluxes during the mean and extreme hot days. Column V: BW plots for the trends in mean SH and LH during the mean and extreme hot days. Column VI: BW plots showing the trend in the evaporative fraction (EF) during mean and extreme hot days. (For interpretation of the references to color in this figure legend, the reader is referred to the web version of this article.)

experiencing extreme temperatures than during the average summer days.

The partitioning of turbulent heat fluxes can be understood in terms of either Bowen ratio ($BR = SH/LH$) or evaporative fraction ($EF = LH/[LH + SH]$). Enhanced partitioning of turbulent fluxes towards sensible heat flux leads to a higher Bowen ratio or a lower evaporative fraction. We use evaporative fraction (EF) because Bowen ratio becomes unbounded in regions where latent heat flux is zero (Donat et al., 2017). We first calculate the EF at each grid point for all summer (JJA) days. Then, we calculate the mean EF for mean summer days (TXm days) and the extreme hot day (TXx day) in a year. Finally, trends in the mean and extreme EF are calculated. A positive trend in EF suggests that the ratio of sensible-to-latent heat flux decreases over time, while a negative trend in EF indicates that the ratio of sensible-to-latent heat flux increases over time. It is the sensible heat flux that leads to more warming of the atmosphere than the latent heat flux (Seneviratne et al., 2010). Column VI shows trends in the EF. It is apparent that over NAf, WNA, Sib, and EA, the EF has a small positive or a negative trend on both mean and extreme days, with little contrast between mean and extreme days. For ECONUS and EU, the EF has a negative trend on both mean and extreme days, but this *negative* trend is significantly bigger on extreme days relative to the mean, confirming the enhancement of the partitioning of the total flux towards the sensible heat flux during extreme temperature days.

Fig. 9 shows trends in surface fluxes and EF over 2051–2100 in the RCP8.5 simulations. Notably, for all regions except East Asia, future

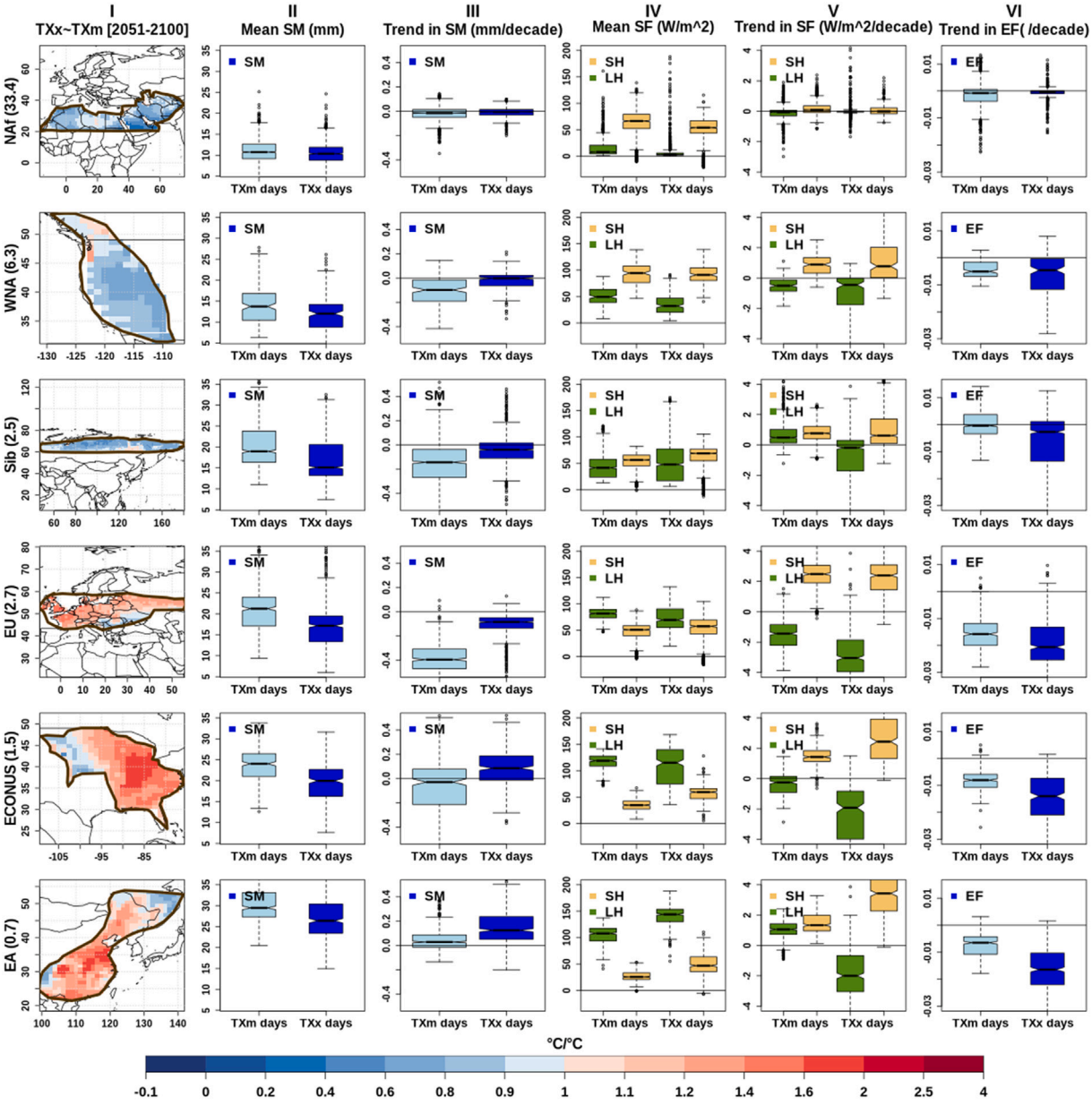

Fig. 9. Same as in Fig. 8 but for the 2051–2100 period.

warming of the extremes relative to the mean remains *broadly* similar to that in the observed period (1979–2021) (column I). For all regions, the future mean soil moisture (column II) and surface fluxes (column IV) during TXm and TXx days remain similar to those in 1979–2021, however, a few noticeable differences occur in trends of those variables. For example, over EU, the trend in LH during TXm days (column V) reverses its sign from positive in 1979–2021 to a negative in 2051–2100, consistent with the increased negative trend in SM (column III). On the other hand, trends in the mean LH and SH change from negative in 1979–2021 to positive in 2051–2100 over EA (column V). As explained before, it is the partitioning of total fluxes into sensible and latent heat during the mean and extreme hot days that matters for relative warming of the extremes relative to the mean. As observed for the 1979–2021 period, trends in EF change little from mean to extreme days for hyper-arid, arid, and semi-arid regions (NAf, WNA, Sib), but decrease more significantly during TXx days than during mean days for dry-subhumid regions (EU and ECONUS). The large interquartile range (IQR) in trends of EF for WNA and Sib is attributed to the regions (northern areas of WNA and western and southern areas in Sib) where TXx is supposed to rise faster than Txm in future warming. Interestingly, future warming of hot extremes is faster than the summer mean daily maximum over EA. This altered nature (reversal of sign) of the relative warming of the extremes is possibly due to the enhanced aridity in the central parts of the EA as indicated in Fig. 7, but may also be connected to other local factors such as changes in large scale circulation patterns and land-sea temperature contrast, not examined in this study. Fig. 10 summarizes the thermodynamical mechanism involved in the land–atmosphere interactions driving the warming of the extreme temperatures relative to the mean.

In summary, in the regions that are either very dry (WNA, NAf) or very wet (EA), surface fluxes are not sensitive to changes in the local soil moisture; thus, there is little or no local soil moisture coupling that supports enhanced warming during extremes than the local mean. In contrast, in regions where soil moisture responds to changes in temperature via changes in the partitioning of the surface fluxes (ECONUS and EU), extreme temperatures increase faster than the mean via suppressed evapotranspiration (or decreased EF) on extreme temperature days.

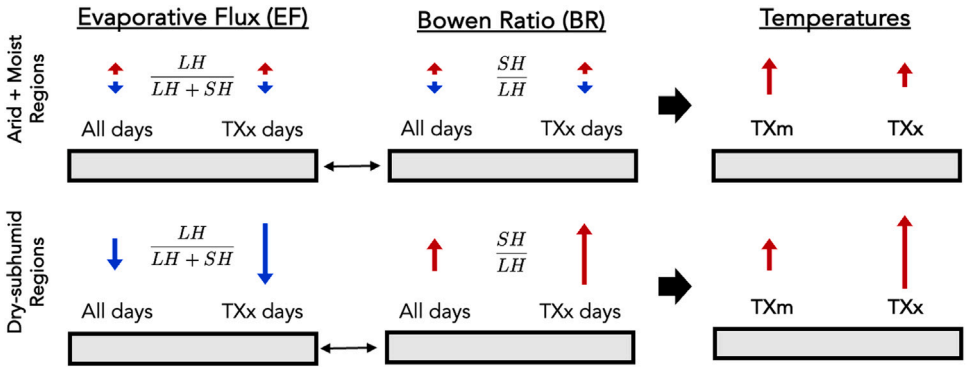

Fig. 10. The infographic shows the role of land–atmosphere interactions in driving the warming of extreme temperatures relative to the mean. The red (blue) arrows indicate positive (negative) trends. The length of the arrows indicates the magnitude of the trend. The top panel shows that where trends in EF (or equivalently, trends in Bowen Ratio) during mean and extreme days are small and comparable in magnitude, the TXx has a smaller positive trend than TXm. This thermodynamical mechanism is generally true for hyper-arid, arid, semi-arid, and moist regions (during 1979–2021); the one exception is East Asia (EA) in the RCP8.5 2051–2100 period, which is a moist region but behaves more like an intermediate region (discussed in text). The bottom panel shows that where trends in EF are significantly more negative on TXx days (or equivalently, where trends in Bowen Ratio are significantly higher), the TXx has a bigger positive trend than TXm. This mechanism holds for dry-subhumid regions and EA (in the RCP8.5 2051–2100 period). (For interpretation of the references to color in this figure legend, the reader is referred to the web version of this article.)

4. Summary

In this work, we estimate trends in the summertime extreme and mean temperatures in the Northern Hemisphere. Our observational analysis uses ERA5 reanalysis over the 1979–2021 period. Our model analysis uses CESM1-LE simulations over the 1979–2021 (historical simulation over 1979–2005 + RCP8.5 simulations over 2006–2021) and 2051–2100 periods (future RCP8.5 simulations). We use the JJA maxima of the daily maximum temperatures to represent temperature extremes (TXx) and JJA means of the daily maximum temperatures to represent mean temperatures (TXm). We compare the warming of extremes relative to the mean in a statistically rigorous generalized extreme value (GEV) distribution approach. We then relate the regional warming patterns of extremes to the local mean by the trends in the surface latent and sensible heat fluxes and evaporative fraction. The trends are examined for the JJA mean and for the day when the extreme hot day in a calendar year occurs.

We find that CESM1-LE and ERA5 show warming trends in both the TXx and TXm over the NH for the 1979–2021 period, except that ERA5 shows a slight negative trend in TXx (i.e., a warming hole) over the eastern CONUS. The CESM1-LE shows accelerated warming of both the mean and extreme temperatures over 2051–2100 in the RCP8.5 simulations. The negative TXx trend over eastern CONUS in ERA5 is consistent with the model-simulated warming trend in TXx, as the warming hole over ECONUS occurs in a few of the CESM1-LE ensemble members. Similar warming holes are randomly distributed in space across the individual simulations. There are several caveats to this result: in addition to the internal climate variability, factors such as land-use intensification (Alter et al., 2018), changes in anthropogenic aerosols (Banerjee et al., 2017), and indirect response to greenhouse gas forcings (Eischeid et al., 2023) may be responsible for the TXx warming hole (Labe et al., 2024). Meehl et al. (2012, 2015) showed that the warming hole exhibited by few models was connected to the Interdecadal Pacific Oscillation (IPO). The degree to which CESM1-LE ensembles simulate these factors/ mechanisms needs to be established.

Changes in TXx relative to the changes in TXm in ERA5 are estimated using a GEV distribution framework, in which the TXm is fitted as a covariate in the location parameter of TXx. The analysis indicates that summertime extreme temperatures are rising slower than the local mean temperatures over most of the Northern Hemisphere during 1979–2021, except in a few regions such as the eastern Contiguous United States (ECONUS) and Northwestern Europe, where extremes are rising faster than the local mean. This spatially differential warming pattern is robust, in the sense that it is simulated by most of the CESM1-LE ensembles in the 1979–2021 period and *broadly* persists through the 2051–2100 RCP8.5 warming period with slight changes in the warming pattern.

We also investigate if the warming pattern of extreme temperatures against the mean is driven by the local hydroclimate defined in terms of aridity index (AI). TXx is shown to be rising faster than TXm in dry-subhumid regions ($1 < AI \leq 2$; eastern CONUS and Europe), and rising slower in hyper-arid ($AI > 10$; North Africa), arid ($5 < AI \leq 10$; Western North America), semi-arid ($2 < AI \leq 5$; Siberia) and humid regions ($AI \leq 1$; East Asia). We explain the relative warming patterns using trends in the partitioning of surface fluxes between latent and sensible heat, measured as evaporative fraction (EF = LH/[SH+LH]). Our investigation suggests that in hyper-arid, arid, semi-arid, and moist regions, trends in EF change little from mean to extreme hot days; whereas in dry-subhumid regions, the trend in EF reduces significantly from mean to extreme heat days. To summarize, TXx rises slower in regions where trends in the partitioning of surface fluxes change little from mean to extreme hot days. On the other hand, TXx rises faster in regions where trends in the partitioning of surface fluxes toward sensible heat during extreme hot days are significantly larger than those during mean days. The results are consistent with the first-order land–atmosphere interaction in the conceptual evapotranspiration regimes described in Fig. 5 of Seneviratne et al. (2010), in that the evaporative fraction is independent of the soil moisture content in the dry (water-limited) and wet (energy-limited) regimes, but responds to changes in soil moisture in the transitional regime between the dry and wet regimes.

The results present in this work are novel in several aspects. First, we show that simple methods based upon the ratio (or difference) of trends in the extreme and mean temperatures may not isolate the warming pattern of extreme hot days relative to the mean in regions where trends are too small. A regression-based approach (using a GEV framework) is a direct method of comparing the changes in extremes against the means. Second, we show that the observed cooling of extreme temperatures over the eastern CONUS can be explained from internal variability (though, we do not rule out the role of the other plausible mechanisms involved), and that the model examined in the study is consistent with observations. Third, our approach shows that the warming of the Northern Hemisphere summertime extreme hot days relative to the mean has a robust pattern across observations and models. The relative warming of the extreme temperatures depends upon the local hydroclimate, which determines the partitioning of the net radiation into sensible and latent heat flux during mean and extreme heat days. These results are consistent with the seminal work of Koster et al. (2009), who identified different responses of the partitioning of sensible and latent heat to the surface/soil characteristics

that control evaporative regimes at each location. A visual comparison of Fig. 5(a) of Koster et al. (2009) and Fig. 7(a) of this manuscript indicates some similarities of the regimes. For example, our hyper-arid North Africa (AI 36.1) and arid coastal western CONUS (AI 6.7) regions match the regions "A" of Koster et al. (2009) identified as the regions where the interannual variability in soil-moisture is simply too small to directly affect the temperature interannual variability. Similarly, our dry sub-humid eastern CONUS region (AI 1.4) geographically matches the regions "B" and "C" identified by Koster et al. (2009) as typically, or frequently, under a soil moisture-controlled regime. However, some dissimilarities also arise between the two studies. For example, the semi-arid Siberian (AI 2.3) and humid East Asia (AI 0.7) regions in our work do not match the energy-controlled ("D") nor the straddled evaporative ("C") regimes expected by Koster et al. (2009), respectively. A proper investigation of the underlying causes behind the similarities and dissimilarities of the hydrological regimes identified in the two studies is out of the scope of this work. We acknowledge the limitations of this study, as only the role of local heat fluxes in determining the warming patterns of extreme temperatures relative to the mean is examined. Other mechanisms such as large-scale atmospheric patterns, land–ocean contrasts, and external factors such as land use change are not investigated. We plan to analyze these aspects in the future.

CRediT authorship contribution statement

Abhishekh Kumar Srivastava: Conceptualization, Data curation, Formal analysis, Investigation, Methodology, Software, Validation, Visualization, Writing – original draft, Writing – review & editing. **Michael Wehner:** Conceptualization, Investigation, Writing – original draft, Writing – review & editing. **Céline Bonfils:** Investigation, Writing – original draft, Writing – review & editing. **Paul Aaron Ullrich:** Funding acquisition, Investigation, Project administration, Supervision, Writing – original draft, Writing – review & editing. **Mark Risser:** Formal analysis, Writing – original draft, Writing – review & editing.

Declaration of competing interest

The authors declare that they have no known competing financial interests or personal relationships that could have appeared to influence the work reported in this paper.

Data availability

The ERA5 data is publicly available on https://www.ecmwf.int/en/forecasts/dataset/ecmwf-reanalysis-v5. The CESM1-LE data analyzed in this study can be downloaded from https://www.cesm.ucar.edu/community-projects/lens.

Declaration of Generative AI and AI-assisted technologies in the writing process

During the preparation of this work the authors used no generative AI and AI-assisted technologies.

Acknowledgments

This research was supported by the Office of Science, Office of Biological and Environmental Research of the US Department of Energy under contract no. DE-AC02-05CH11231 for the CASCADE Scientific Focus (funded by the Regional and Global Model Analysis Program area within the Earth and Environmental Systems Modeling Program). The work of C.B. and of P.A.U. is supported by the "PCMDI: An Earth System Model Evaluation Project" Science Focus Area (SFA) funded through the Regional and Global Climate Modeling Program of the Office of Science at the DOE, and is performed under the auspices of the U.S. Department of Energy by Lawrence Livermore National Laboratory under contract DE-AC52-07NA27344. We thank Prof. Timothy DelSole of George Mason University, Fairfax, VA, USA for his valuable suggestions on the statistical analysis.

Appendix A. Supplementary data

Supplementary material related to this article can be found online at https://doi.org/10.1016/j.wace.2024.100709.

References

Alexander, L.V., Zhang, X., Peterson, T.C., Caesar, J., Gleason, B., Klein Tank, A.M.G., Haylock, M., Collins, D., Trewin, B., Rahimzadeh, F., Tagipour, A., Rupa Kumar, K., Revadekar, J., Griffiths, G., Vincent, L., Stephenson, D.B., Burn, J., Aguilar, E., Brunet, M., Taylor, M., New, M., Zhai, P., Rusticucci, M., Vazquez-Aguirre, J.L., 2006. Global observed changes in daily climate extremes of temperature and precipitation. J. Geophys. Res.: Atmos. 111 (D5), http://dx.doi.org/10.1029/2005JD006290.

Alter, R.E., Douglas, H.C., Winter, J.M., Eltahir, E.A.B., 2018. Twentieth Century Regional climate change during the summer in the central United States attributed to agricultural intensification. Geophys. Res. Lett. 45 (3), 1586–1594. http://dx.doi.org/10.1002/2017GL075604.

Banerjee, A., Polvani, L.M., Fyfe, J.C., 2017. The United States "warming hole": Quantifying the forced aerosol response given large internal variability. Geophys. Res. Lett. 44 (4), 1928–1937. http://dx.doi.org/10.1002/2016GL071567.

Benson, D.O., Dirmeyer, P.A., 2021. Characterizing the relationship between temperature and soil moisture extremes and their role in the exacerbation of heat waves over the contiguous United States. J. Clim. 34 (6), 2175–2187. http://dx.doi.org/10.1175/JCLI-D-20-0440.1.

Byrne, M.P., 2021. Amplified warming of extreme temperatures over tropical land. Nat. Geosci. 14 (11), 837–841. http://dx.doi.org/10.1038/s41561-021-00828-8.

Christidis, N., Stott, P.A., Brown, S.J., 2011. The role of human activity in the recent warming of extremely warm daytime temperatures. J. Clim. 24 (7), 1922–1930. http://dx.doi.org/10.1175/2011JCLI4150.1.

Cohen, J.L., Furtado, J.C., Barlow, M., Alexeev, V.A., Cherry, J.E., 2012. Asymmetric seasonal temperature trends. Geophys. Res. Lett. 39 (4), http://dx.doi.org/10.1029/2011GL050582.

Coles, S., Bawa, J., Trenner, L., Dorazio, P., 2001. An Introduction to Statistical Modeling of Extreme Values, vol. 208, Springer, http://dx.doi.org/10.1007/978-1-4471-3675-0.

Cowan, T., Hegerl, G.C., Schurer, A., Tett, S.F.B., Vautard, R., Yiou, P., Jézéquel, A., Otto, F.E.L., Harrington, L.J., Ng, B., 2020. Ocean and land forcing of the record-breaking dust bowl heatwaves across central United States. Nature Commun. 11 (1), 2870. http://dx.doi.org/10.1038/s41467-020-16676-w.

Denissen, J.M., Teuling, A.J., Pitman, A.J., Koirala, S., Migliavacca, M., Li, W., Reichstein, M., Winkler, A.J., Zhan, C., Orth, R., 2022. Widespread shift from ecosystem energy to water limitation with climate change. Nature Clim. Change 12 (7), 677–684. http://dx.doi.org/10.1038/s41558-022-01403-8.

Di Luca, A., de Elía, R., Bador, M., Argüeso, D., 2020. Contribution of mean climate to hot temperature extremes for present and future climates. Weather Clim. Extremes 28, 100255. http://dx.doi.org/10.1016/j.wace.2020.100255.

Diffenbaugh, N.S., Ashfaq, M., 2010. Intensification of hot extremes in the United States. Geophys. Res. Lett. 37 (15), http://dx.doi.org/10.1029/2010GL043888.

Diffenbaugh, N.S., Singh, D., Mankin, J.S., Horton, D.E., Swain, D.L., Touma, D., Charland, A., Liu, Y., Haugen, M., Tsiang, M., Rajaratnam, B., 2017. Quantifying the influence of global warming on unprecedented extreme climate events. Proc. Natl. Acad. Sci. 114 (19), 4881–4886. http://dx.doi.org/10.1073/pnas.1618082114.

Donat, M.G., Pitman, A.J., Seneviratne, S.I., 2017. Regional warming of hot extremes accelerated by surface energy fluxes. Geophys. Res. Lett. 44 (13), 7011–7019. http://dx.doi.org/10.1002/2017GL073733.

Duan, S.Q., Findell, K.L., Wright, J.S., 2020. Three regimes of temperature distribution change over dry land, moist land, and oceanic surfaces. Geophys. Res. Lett. 47 (24), http://dx.doi.org/10.1029/2020GL090997, e2020GL090997 2020GL090997.

Dunn, R.J.H., Alexander, L.V., Donat, M.G., Zhang, X., Bador, M., Herold, N., Lippmann, T., Allan, R., Aguilar, E., Barry, A.A., Brunet, M., Caesar, J., Chagnaud, G., Cheng, V., Cinco, T., Durre, I., de Guzman, R., Htay, T.M., Wan Ibadullah, W.M., Bin Ibrahim, M.K.I., Khoshkam, M., Kruger, A., Kubota, H., Leng, T.W., Lim, G., Li-Sha, L., Marengo, J., Mbatha, S., McGree, S., Menne, M., de los Milagros Skansi, M., Ngwenya, S., Nkrumah, F., Oonariya, C., Pabon-Caicedo, J.D., Panthou, G., Pham, C., Rahimzadeh, F., Ramos, A., Salgado, E., Salinger, J., Sané, Y., Sopaheluwakan, A., Srivastava, A., Sun, Y., Timbal, B., Trachow, N., Trewin, B., van der Schrier, G., Vazquez-Aguirre, J., Vasquez, R., Villarroel, C., Vincent, L., Vischel, T., Vose, R., Bin Hj Yussof, M.N., 2020. Development of an updated global land in situ-based data set of temperature and precipitation extremes: HadEX3. J. Geophys. Res.: Atmos. 125 (16), http://dx.doi.org/10.1029/2019JD032263, e2019JD032263 10.1029/2019JD032263.

Ebi, K.L., Capon, A., Berry, P., Broderick, C., de Dear, R., Havenith, G., Honda, Y., Kovats, R.S., Ma, W., Malik, A., Morris, N.B., Nybo, L., Seneviratne, S.I., Vanos, J., Jay, O., 2021. Hot weather and heat extremes: Health risks. Lancet 398 (10301), 698–708. http://dx.doi.org/10.1016/S0140-6736(21)01208-3.

Eischeid, J.K., Hoerling, M.P., Quan, X.-W., Kumar, A., Barsugli, J., Labe, Z.M., Kunkel, K.E., Schreck, C.J., Easterling, D.R., Zhang, T., Uehling, J., Zhang, X., 2023. Why has the summertime central U.S. warming hole not disappeared? J. Clim. 36 (20), 7319–7336. http://dx.doi.org/10.1175/JCLI-D-22-0716.1.

Hausfather, Z., Peters, G.P., 2020. Emissions–The 'Business as Usual' story Is Misleading. Nature, http://dx.doi.org/10.1038/d41586-020-00177-3.

Hersbach, H., Bell, B., Berrisford, P., Hirahara, S., Horányi, A., Muñoz-Sabater, J., Nicolas, J., Peubey, C., Radu, R., Schepers, D., Simmons, A., Soci, C., Abdalla, S., Abellan, X., Balsamo, G., Bechtold, P., Biavati, G., Bidlot, J., Bonavita, M., De Chiara, G., Dahlgren, P., Dee, D., Diamantakis, M., Dragani, R., Flemming, J., Forbes, R., Fuentes, M., Geer, A., Haimberger, L., Healy, S., Hogan, R.J., Hólm, E., Janisková, M., Keeley, S., Laloyaux, P., Lopez, P., Lupu, C., Radnoti, G., de Rosnay, P., Rozum, I., Vamborg, F., Villaume, S., Thépaut, J.-N., 2020. The ERA5 global reanalysis. Q. J. R. Meteorol. Soc. 146 (730), 1999–2049. http://dx.doi.org/10.1002/qj.3803.

Hsu, H., Dirmeyer, P.A., 2023. Soil moisture-evaporation coupling shifts into new gears under increasing CO2. Nature Commun. 14 (1), 1162. http://dx.doi.org/10.1038/s41467-023-36794-5.

Jones, P.W., 1999. First- and second-order conservative remapping schemes for grids in spherical coordinates. Mon. Weather Rev. 127 (9), 2204–2210. http://dx.doi.org/10.1175/1520-0493(1999)127<2204:FASOCR>2.0.CO;2.

Kay, J.E., Deser, C., Phillips, A., Mai, A., Hannay, C., Strand, G., Arblaster, J.M., Bates, S.C., Danabasoglu, G., Edwards, J., Holland, M., Kushner, P., Lamarque, J.-F., Lawrence, D., Lindsay, K., Middleton, A., Munoz, E., Neale, R., Oleson, K., Polvani, L., Vertenstein, M., 2015. The Community Earth System Model (CESM) large ensemble project: A community resource for studying climate change in the presence of internal climate variability. Bull. Am. Meteorol. Soc. 96 (8), 1333–1349. http://dx.doi.org/10.1175/BAMS-D-13-00255.1.

Koster, R.D., Schubert, S.D., Suarez, M.J., 2009. Analyzing the concurrence of meteorological droughts and warm periods, with implications for the determination of evaporative regime. J. Clim. 22 (12), 3331–3341. http://dx.doi.org/10.1175/2008JCLI2718.1.

Krakauer, N.Y., 2023. Amplification of extreme hot temperatures over recent decades. Climate 11 (2), http://dx.doi.org/10.3390/cli11020042.

Kunkel, K.E., Liang, X.-Z., Zhu, J., Lin, Y., 2006. Can CGCMs simulate the twentieth-century "warming hole" in the central United States? J. Clim. 19 (17), 4137–4153. http://dx.doi.org/10.1175/JCLI3848.1.

Labe, Z.M., Johnson, N.C., Delworth, T.L., 2024. Changes in United States summer temperatures revealed by explainable neural networks. Earth's Future 12 (2), http://dx.doi.org/10.1029/2023EF003981, e2023EF003981 2023EF003981.

Leibensperger, E.M., Mickley, L.J., Jacob, D.J., Chen, W.-T., Seinfeld, J.H., Nenes, A., Adams, P.J., Streets, D.G., Kumar, N., Rind, D., 2012. Climatic effects of 1950–2050 changes in US anthropogenic aerosols – Part 2: Climate response. Atmos. Chem. Phys. 12 (7), 3349–3362. http://dx.doi.org/10.5194/acp-12-3349-2012.

Lewis, S.C., King, A.D., 2017. Evolution of mean, variance and extremes in 21st century temperatures. Weather Clim. Extremes 15, 1–10. http://dx.doi.org/10.1016/j.wace.2016.11.002.

Li, C., Zwiers, F., Zhang, X., Li, G., Sun, Y., Wehner, M., 2021. Changes in annual extremes of daily temperature and precipitation in CMIP6 models. J. Clim. 34 (9), 3441–3460. http://dx.doi.org/10.1175/JCLI-D-19-1013.1.

Lian, X., Huang, J., Li, H., He, Y., Ouyang, Z., Fu, S., Zhao, Y., Wang, D., Wang, R., Guan, X., 2023. Heat waves accelerate the spread of infectious diseases. Environ. Res. 231, 116090. http://dx.doi.org/10.1016/j.envres.2023.116090, https://www.sciencedirect.com/science/article/pii/S0013935123008824.

McKinnon, K.A., Rhines, A., Tingley, M.P., Huybers, P., 2016. The changing shape of northern hemisphere summer temperature distributions. J. Geophys. Res.: Atmos. 121 (15), 8849–8868. http://dx.doi.org/10.1002/2016JD025292.

Meehl, G.A., Arblaster, J.M., Branstator, G., 2012. Mechanisms contributing to the warming hole and the consequent U.S. East–West differential of heat extremes. J. Clim. 25 (18), 6394–6408. http://dx.doi.org/10.1175/JCLI-D-11-00655.1.

Meehl, G.A., Arblaster, J.M., Chung, C.T.Y., 2015. Disappearance of the southeast U.S. "warming hole" with the late 1990s transition of the interdecadal Pacific oscillation. Geophys. Res. Lett. 42 (13), 5564–5570. http://dx.doi.org/10.1002/2015GL064586.

Meehl, G.A., Tebaldi, C., 2004. More intense, more frequent, and longer lasting heat waves in the 21st century. Science 305 (5686), 994–997. http://dx.doi.org/10.1126/science.1098704.

Miller, S., Chua, K., Coggins, J., Mohtadi, H., 2021. Heat waves, climate change, and economic output. J. Eur. Econom. Assoc. 19 (5), 2658–2694. http://dx.doi.org/10.1093/jeea/jvab009.

Miller, N.L., Hayhoe, K., Jin, J., Auffhammer, M., 2008. Climate, extreme heat, and electricity demand in California. J. Appl. Meteorol. Climatol. 47 (6), 1834–1844. http://dx.doi.org/10.1175/2007JAMC1480.1.

Min, S.-K., Zhang, X., Zwiers, F., Shiogama, H., Tung, Y.-S., Wehner, M., 2013. Multimodel detection and attribution of extreme temperature changes. J. Clim. 26 (19), 7430–7451. http://dx.doi.org/10.1175/JCLI-D-12-00551.1.

Miralles, D.G., Gentine, P., Seneviratne, S.I., Teuling, A.J., 2019. Land–atmospheric feedbacks during droughts and heatwaves: state of the science and current challenges. Ann. New York Acad. Sci. 1436 (1), 19–35. http://dx.doi.org/10.1111/nyas.13912.

Miralles, D.G., Teuling, A.J., van Heerwaarden, C.C., Vilà-Guerau de Arellano, J., 2014. Mega-heatwave temperatures due to combined soil desiccation and atmospheric heat accumulation. Nat. Geosci. 7 (5), 345–349. http://dx.doi.org/10.1038/ngeo2141.

Partridge, T.F., Winter, J.M., Osterberg, E.C., Hyndman, D.W., Kendall, A.D., Magilligan, F.J., 2018. Spatially distinct seasonal patterns and forcings of the U.S. warming hole. Geophys. Res. Lett. 45 (4), 2055–2063. http://dx.doi.org/10.1002/2017GL076463.

Patterson, M., 2023. North-west europe hottest days are warming twice as fast as mean summer days. Geophys. Res. Lett. 50 (10), http://dx.doi.org/10.1029/2023GL102757, e2023GL102757 2023GL102757.

Perkins, S.E., Alexander, L.V., Nairn, J.R., 2012. Increasing frequency, intensity and duration of observed global heatwaves and warm spells. Geophys. Res. Lett. 39 (20), http://dx.doi.org/10.1029/2012GL053361.

Philip, S.Y., Kew, S.F., van Oldenborgh, G.J., Anslow, F.S., Seneviratne, S.I., Vautard, R., Coumou, D., Ebi, K.L., Arrighi, J., Singh, R., van Aalst, M., Pereira Marghidan, C., Wehner, M., Yang, W., Li, S., Schumacher, D.L., Hauser, M., Bonnet, R., Luu, L.N., Lehner, F., Gillett, N., Tradowsky, J.S., Vecchi, G.A., Rodell, C., Stull, R.B., Howard, R., Otto, F.E.L., 2022. Rapid attribution analysis of the extraordinary heat wave on the Pacific coast of the US and Canada in June 2021. Earth Syst. Dynam. 13 (4), 1689–1713. http://dx.doi.org/10.5194/esd-13-1689-2022.

Seneviratne, S.I., Corti, T., Davin, E.L., Hirschi, M., Jaeger, E.B., Lehner, I., Orlowsky, B., Teuling, A.J., 2010. Investigating soil moisture–climate interactions in a changing climate: A review. Earth-Sci. Rev. 99 (3), 125–161. http://dx.doi.org/10.1016/j.earscirev.2010.02.004.

Seneviratne, S.I., Donat, M.G., Pitman, A.J., Knutti, R., Wilby, R.L., 2016. Allowable CO2 emissions based on regional and impact-related climate targets. Nature 529 (7587), 477–483. http://dx.doi.org/10.1038/nature16542.

Seneviratne, S.I., Hauser, M., 2020. Regional climate sensitivity of climate extremes in CMIP6 versus CMIP5 multimodel ensembles. Earth's Future 8 (9), http://dx.doi.org/10.1029/2019EF001474, e2019EF001474 2019EF001474.

Seneviratne, S.I., Zhang, X., Adnan, M., Badi, W., Dereczynski, C., Di Luca, A., Ghosh, S., Iskandar, I., Kossin, J., Lewis, S., Otto, F., Pinto, I., Satoh, M., Vicente-Serrano, S.M., Wehner, M., Zhou, B., 2021. 2021: Weather and climate extreme events in a changing climate. In: Zhai, V.P., Pirani, A., Connors, S.L., Péan, C., Berger, S., Caud, N., Chen, Y., Goldfarb, L., Gomis, M.I., Huang, M., Leitzell, K., Lonnoy, E., Matthews, J.B.R., Maycock, T.K., Waterfield, T., ci, O.Y., Yu, R., Zhou, B. (Eds.), Climate Change 2021: the Physical Science Basis. Contribution of Working Group I to the Sixth Assessment Report of the Intergovernmental Panel on Climate Change[masson-Delmotte. Cambridge University Press, Cambridge, United Kingdom and New York, NY, USA, pp. 1513–1766.

Sun, C., Zhu, L., Liu, Y., Wei, T., Guo, Z., 2022. CMIP6 model simulation of concurrent continental warming holes in Eurasia and North America since 1990 and their relation to the Indo-Pacific SST warming. Glob. Planet. Change 213, 103824. http://dx.doi.org/10.1016/j.gloplacha.2022.103824.

Tebaldi, C., Arblaster, J.M., Knutti, R., 2011. Mapping model agreement on future climate projections. Geophys. Res. Lett. 38 (23), http://dx.doi.org/10.1029/2011GL049863.

Thiery, W., Davin, E.L., Lawrence, D.M., Hirsch, A.L., Hauser, M., Seneviratne, S.I., 2017. Present-day irrigation mitigates heat extremes. J. Geophys. Res.: Atmos. 122 (3), 1403–1422. http://dx.doi.org/10.1002/2016JD025740.

Tollefson, J., 2020. How hot will Earth get by 2100. Nature 580 (7804), 443–445. http://dx.doi.org/10.1038/d41586-020-01125-x.

Vogel, M.M., Orth, R., Cheruy, F., Hagemann, S., Lorenz, R., van den Hurk, B.J.J.M., Seneviratne, S.I., 2017. Regional amplification of projected changes in extreme temperatures strongly controlled by soil moisture-temperature feedbacks. Geophys. Res. Lett. 44 (3), 1511–1519. http://dx.doi.org/10.1002/2016GL071235.

Vose, R.S., Easterling, D.R., Kunkel, K.E., LeGrande, A.N., Wehner, M.F., 2017. 2017: Temperature changes in the United States. In: [Wuebbles, V.I., J., D., Fahey, D.W., Hibbard, K.A., Dokken, D.J., Stewart, B.C., Maycock, T.K. (Eds.), In: Climate Science Special Report: Fourth National Climate Assessment, vol. I, U.S. Global Change Research Program, Washington, DC, USA, pp. 185–206. http://dx.doi.org/10.7930/J0N29V45.

Wang, R., Gentine, P., Li, L., Chen, J., Ning, L., Yuan, L., Lü, G., 2022. Observational evidence of regional increasing hot extreme accelerated by surface energy partitioning. J. Hydrometeorol. 23 (3), 491–501. http://dx.doi.org/10.1175/JHM-D-21-0114.1.

Wankar, A.K., Rindhe, S.N., Doijad, N.S., 2021. Heat stress in dairy animals and current milk production trends, economics, and future perspectives: The global scenario. Trop. Anim. Health Prod. 53 (1), 70. http://dx.doi.org/10.1007/s11250-020-02541-x.

Wehner, M.F., 2020. Characterization of long period return values of extreme daily temperature and precipitation in the CMIP6 models: Part 2, projections of future change. Weather Clim. Extremes 30, 100284. http://dx.doi.org/10.1016/j.wace.2020.100284.

Wehner, M., Stone, D., Mitchell, D., Shiogama, H., Fischer, E., Graff, L.S., Kharin, V.V., Lierhammer, L., Sanderson, B., Krishnan, H., 2018a. Changes in extremely hot days under stabilized 1.5 and 2.0 °C global warming scenarios as simulated by the HAPPI multi-model ensemble. Earth Syst. Dynam. 9 (1), 299–311. http://dx.doi.org/10.5194/esd-9-299-2018.

Wehner, M., Stone, D., Shiogama, H., Wolski, P., Ciavarella, A., Christidis, N., Krishnan, H., 2018b. Early 21st century anthropogenic changes in extremely hot days as simulated by the C20C+ detection and attribution multi-model ensemble. Weather Clim. Extremes 20, 1–8. http://dx.doi.org/10.1016/j.wace.2018.03.001.

Whan, K., Zscheischler, J., Orth, R., Shongwe, M., Rahimi, M., Asare, E.O., Seneviratne, S.I., 2015. Impact of soil moisture on extreme maximum temperatures in Europe. Weather Clim. Extremes 9, 57–67. http://dx.doi.org/10.1016/j.wace.2015.05.001, The World Climate Research Program Grand Challenge on Extremes – WCRP-ICTP Summer School on Attribution and Prediction of Extreme Events.

Zomer, R.J., Xu, J., Trabucco, A., 2022. Version 3 of the global aridity index and potential evapotranspiration database. Sci. Data 9 (1), 409. http://dx.doi.org/10.1038/s41597-022-01493-1.

Zwiers, F.W., Zhang, X., Feng, Y., 2011. Anthropogenic influence on long return period daily temperature extremes at regional scales. J. Clim. 24 (3), 881–892. http://dx.doi.org/10.1175/2010JCLI3908.1.